frontiers in Materials

ORIGINAL RESEARCH
published: 07 March 2017
doi: 10.3389/fmats.2017.00005

Influence of Cooling Rate on Cracking and Plastic Deformation during Impact and Indentation of Borosilicate Glasses

Christoffer Zehnder[1†], Sebastian Bruns[2†], Jan-Niklas Peltzer[1], Karsten Durst[2], Sandra Korte-Kerzel[1] and Doris Möncke[3,4‡]*

[1] Institut für Metallkunde und Metallphysik, RWTH Aachen University, Aachen, Germany, [2] FG Physikalische Metallkunde, Technische Universität Darmstadt, Darmstadt, Germany, [3] Otto Schott Institute of Materials Research, Friedrich Schiller University, Jena, Germany, [4] Theoretical and Physical Chemistry Institute, National Hellenic Research Foundation, Athens, Greece

OPEN ACCESS

Edited by:
Ashutosh Goel,
Rutgers University, USA

Reviewed by:
Pathikumar Sellappan,
University of California San Diego, USA
Charles Robert Kurkjian,
Retired, USA

****Correspondence:***
Sebastian Bruns
s.bruns@phm.tu-darmstadt.de

[†]These authors have contributed equally to this work.

[‡]Present address:
Doris Möncke,
Inamori School of Engineering, Alfred University, Alfred, NY, USA

Specialty section:
This article was submitted to Glass Science, a section of the journal Frontiers in Materials

Received: *22 December 2016*
Accepted: *17 February 2017*
Published: *07 March 2017*

Citation:
Zehnder C, Bruns S, Peltzer J-N, Durst K, Korte-Kerzel S and Möncke D (2017) Influence of Cooling Rate on Cracking and Plastic Deformation during Impact and Indentation of Borosilicate Glasses. Front. Mater. 4:5. doi: 10.3389/fmats.2017.00005

The influence of a changing glass topology on local mechanical properties was studied in a multitechnique nanomechanical approach. The glass response against sharp contacts can result in structural densification, plastic flow, or crack initiation. By using instrumented indentation testing, the mechanical response was studied in different strain rate regimes for a sodium borosilicate glass (NBS) exhibiting altering structures due to varying processing conditions. Comparison with data from former studies and with literature data on other glass structures helped to elucidate the role of the borate and silicate subnetworks and to understand the overall mechanical properties of the mixed glass systems. A peculiarity of some of the NBS glasses tested in this study is the fact that the connectivity of the borate and silicate entities depends on the sample's thermal history. Although the influence on macroscopic material properties such as E and H is minor, the onset of cracking indeed is influenced by those structural changes within the glass. Rapidly quenched glass shows an improved crack resistance, which is even more pronounced at high strain rates. Studies on various processing conditions further indicate that this transition is closely related to the cooling rate around T_g. The strain rate dependence of cracking is discussed in terms of the occurrence of shear deformation and densification.

Keywords: borosilicate glasses, indentation, impact, interconnectivity, deformation mechanism, strain rate sensitivity, activation volume

INTRODUCTION

Shear- and Densification-Driven Deformation in Fully Polymerized Borate and Borosilicate Glasses

Glasses generally can be categorized into two groups, anomalous and normal glass. The term anomalous behavior was coined for vitreous silica, which showed a densification ability up to 20%, a contrary behavior against mechanical impact as most other glasses (Arora et al., 1979; Barlet et al., 2015). However, silica remains perhaps the most studied glass, and other commercially important

silica rich glasses fall into this category as well, including ultralow expansion glass (SiO_2–TiO_2) or the low-alkaline borosilicate glasses of the pyrex or duran type. In normal glasses, deformation occurs *via* a shearing process, the crack propagates along non-bridging oxygen ions (nbO), which rearrange to facilitate crack growth. Densification plays a much lesser role for normal than for anomalous glasses. This can be explained by a higher packing density in these glasses where modifier cations near nbO atoms, as well as charge compensating cations in the vicinity of $[BO_4]^-$ tetrahedra, fill voids, which in the fully polymerized silica glass ensue from a network made up predominantly from 5- and 6-membered rings.

The focus of this project was on low-alkaline borosilicate glasses (Winterstein-Beckmann et al., 2014a,b; Malchow et al., 2015). NBS2 belong to silica-rich but low-alkali borosilicate glasses that show densification-driven deformation akin to vitreous silica. In those glasses, Q^4 SiO_4-tetrahedra are replaced by an equally fully connected $[B\emptyset_4]^-$ tetrahedra, which are charge balanced by a Na^+ ion (Vogel, 1994; Möncke and Ehrt, 2002; Möncke et al., 2003, 2006, 2009, 2013). As the SiO_2:B_2O_3 ratio decreases, the glasses show less anomalous densification-driven deformation but more shear-driven deformation despite the fact that these low-alkaline glasses do not contain any significant numbers of nbO (Winterstein-Beckmann et al., 2014b).

Raman spectroscopy shows that the number or borate and boroxol rings decreases significantly upon indentation. Thus, it was suggested (Winterstein-Beckmann et al., 2014b) that a shearing mechanism occurs, which involves the breaking of boroxol rings, e.g., through overcoordination of BO_3 to $[B\emptyset_4]^-$ entities, e.g., when two neighboring boroxol rings are closely facing another. For reasons of charge balance, an overcoordination of oxygen ions from twofold to threefold is also required, a mechanism that has been described for vitreous B_2O_3 under pressure (Lee et al., 2005). Limbach et al. (2015) compiled a review on the mechanical properties of ternary borosilicate glasses comparing their own experimental data with literature values and trying to highlight trends with varying composition and structural variations of these glasses.

The Influence of Cooling Rate on the Connectivity of Sodium Borosilicate (NBS) Glasses

Processing of glasses can change their structure significantly. Such modifications can be reflected in a different coordination of the network former such as boron (Yano et al., 2003a; Zhang and Eckert, 2008; Guerette et al., 2015) or in variations in the distribution of nbO, e.g., the disproportionation of $2Q^2 \leftrightarrows Q^3 + Q^1$ units (Brawer and White, 1975) (Q^n denotes a basic glass forming tetrahedral with n bridging and $4-n$ non-bridging oxygen atoms). Moreover, changes in the connectivity of the network former polyhedra have also been observed (Yano et al., 2003b).

The latter case is well studied for the low-alkali borosilicate glass NBS2 (Möncke and Ehrt, 2002; Möncke et al., 2003, 2006, 2009, 2015). If the melt is rapidly quenched, a high mixing of borate and silicate entities ensues, which is apparent in Raman and IR spectra through higher intensities in bands assigned to mixed B-O-Si stretching and bending modes (Möncke et al., 2006). If the same melt is instead carefully cast and annealed at or above T_g, bands grow in intensity, which are assigned to homopolar bonds, that is, to B-O-B or Si-O-Si bonds, and especially with ring breathing modes of silicate or borate and boroxol rings (Möncke et al., 2006). These results are also confirmed by NMR measurements (Möncke et al., 2003, 2015a,b). Particularly 2D NMR showed very convincingly how mixed B-O-Si bonds decrease upon cooling and that the loss of B^{iv}-O-Si bonds is almost absolute, whereas B^{iii}-O-Si bonds, although decreasing in number, still remain in significant numbers (Roman letters denote the coordination number of boron) (Möncke et al., 2015a,b).

Mechanical Testing of Glass

The local mechanical properties of glasses depend strongly on the glass composition and connectivity, the strain rate, and the indenter geometries used (Youn and Kang, 2005; Rouxel et al., 2014; Morozumi et al., 2016).

In this study, the response of a variety of glasses against different types of mechanical impact is examined. For this, nanoindentation with a Berkovich tip geometry is used to characterize the influence of processing parameters on the mechanical response of NBS glasses. It provides different analysis parameters: Usually, hardness is determined using the Oliver–Pharr technique (Oliver and Pharr, 1992, 2004) and is given by:

$$H = \frac{P_{\max}}{A_c}, \tag{1}$$

where A_c is the contact area under maximum indentation load P_{max}. The reduced indentation modulus E_R is defined as:

$$E_R = \left[\frac{\left(1-\nu^2\right)}{E} + \frac{\left(1-\nu_I^2\right)}{E_I} \right], \tag{2}$$

where ν is Poisson's ratio. The subscript I refers to the diamond indenter properties. In this study, values of E(I) and ν(I) (Oliver and Pharr, 1992) are assumed for E and ν, respectively. For the borosilicates, a Poisson's ratio ν of 0.2 (Limbach et al. 2015) was used for calculation of the elastic modulus.

The directly measurable indentation parameter S^2/P, where S is the unloading stiffness at a load P, offers some benefits compared to the previously presented approach. Material sink-in or pileup strongly influences the contact area A_c in Eq. 1 and thus the associated hardness values. S^2/P in contrast is independent of both the indentation depth and the contact area for bulk, homogeneous materials as glass (Joslin and Oliver, 1990). If Young's modulus E is known, S^2/P can be used to calculate more precise hardness values:

$$\frac{S^2}{P} = \frac{4 \cdot E_R}{\pi \cdot H}. \tag{3}$$

Although, E and H offer a unique way to quickly compare the mechanical response of different materials, it does not allow to directly make statements on the underlying mechanisms. Further analysis methods of the deformed material, on the

other hand, allow to correlate the results of nanoindentation measurements to mechanisms taking place in the material. Indentation with a micro Vickers indenter results in relative large indented areas, which allow to map the structural changes over the indented areas, e.g., by using a Raman microscope with a resolution of 0.5 μm (Winterstein-Beckmann et al., 2014a,b; Malchow et al., 2015). Moreover, indentation testing can also be used to characterize cracking. The approach by Lawn et al. (1980) relates the radial crack length c and the peak load P to the fracture toughness K_{IC}.

The previously presented methods are usually performed at a constant strain rate $\dot{\varepsilon}$. In contrast, glass was already found to be strain rate sensitive (Limbach et al., 2014). Maier et al. (2011) developed a nanoindentation method with implemented jumps in strain rate during the indentation cycle. Strain rate sensitivity becomes visible within just one indentation test in the form of a jump in hardness. The coefficient of strain rate sensitivity m can be calculated according to Mayo and Nix (1988):

$$m_{\text{nanoindentation}} = \frac{d\left(\ln H\right)}{d\left(\ln \dot{\varepsilon}_{\text{indentation}}\right)}. \quad (4)$$

Once m is known, the activation volume V can be calculated according to Maier et al. (2011) and Durst and Maier (2015):

$$V = \frac{\sqrt{3} \cdot k \cdot T}{\sigma_f \cdot m}. \quad (5)$$

The flow stress σ_f relates to the hardness H by the constraint factor $C = H/\sigma_f$, which is assumed to be 1.5 (Swain and Hagan, 1976) in this study.

Although quasi-static indentation can cover strain rates in the order of 2–3 magnitudes, it is limited to values below 10^{-1} s^{-1}. Nanoindentation can be conducted also with an impact module that allows the utilization of strain rates a few orders of magnitude higher than quasi-static indentation. Contrary to microindentation and nanoindentation, which is established as a standard testing technique when mechanical properties of a material are considered (Rouxel et al., 2010; Limbach et al., 2014; Barlet et al., 2015; Yao et al., 2016), nano-impact testing has, up to now, been applied only in few instances (Beake et al., 2001, 2009; Beake and Smith, 2004; Trelewicz and Schuh, 2008; Jennett and Nunn, 2011; Somekawa and Schuh, 2012; Wheeler and Gunner, 2013). The main problem is probably the natural oscillation of the pendulum during the first impact. Analyzing the depth signal in a reliable way is impossible because the actual oscillation due to the impact testing is super positioned on a measuring artifact (Wheeler and Gunner, 2013). Jennett et al. have shown that by applying additional stiffening parts to the pendulum, the natural oscillation can be suppressed sufficiently so that an analyzable signal can be received from this kind of test (Jennett and Nunn, 2011). This stiffening procedure was applied to the system used in this article.

An overview on the studied samples, their composition, and selected properties, as well as the comments on additional methods of mechanical testing discussed in this article, can be found in **Table 1**. Topological changes were considered from the analysis of crack patterns and the degree of densification. The structural variation determined using Raman spectroscopy was taken from previous publications.

TABLE 1 | All glass samples discussed in the current study are listed with their nominal composition and selected properties.

	NBS1	$NBS2_{fc}$	$NBS2_{qu}$	SiO_2
SiO_2	74	**74**	–	100
B_2O_3	10	**20.7**	–	–
Na_2O	16	**4.3**	–	–
Al_2O_3	–	**1**	–	–
Density (g/cm³)[a]	2.45	2.171	2.169	2.20
T_g (K)[b]	823	715	–	1,403
Hardness, H (GPa)[c]	7.52	6.45	–	9.7
E (GPa)[b,c]	78.8	55.7	–	70
E (GPa)[d]	81.6	52.35	–	72.4
Poisson ratio v[b,c]	0.204	0.21	–	0.17
Strain rate sensitivity, m	0.0227	0.0231	–	0.0143
Activation volume V (nm³)	0.0617	0.0713	–	0.0793
Atoms in activation, volume	4	5	–	5

Bold, highlighted the annealed and quenched samples of same composition but different connectivity, discussed in detail in this study.
Comments on additional methods of mechanical testing and additional references are included.
qu, quenched; fc, furnace cooled from T_{mc} = 700°C.
[a]*Taken from the study by Malchow et al. (2015).*
[b]*Taken from the study by Limbach et al. (2015).*
[c]*Determined by ultrasonic echography.*
[d]*Determined by nanoindentation.*

EXPERIMENTS AND METHODS

Samples

The borosilicate glasses NBS1 and NBS2 were prepared in 100 to 250 g batches of optical-grade raw materials SiO_2, Na_2CO_3 and H_3BO_3 in Pt- or Pt-Rh20 crucibles in a conductive heated furnace at melting temperatures T_m of 1,450°C (NBS1) and 1,650 to 1,750°C (NBS2). For the NBS2 glass, Al_2O_3 was added as $Al(OH)_3$ to avoid phase separation.

The melts were poured into preheated graphite molds with a temperature ~50 K above T_g (see also **Table 1**) and cooled down to room temperature in a furnace with a cooling rate of 30 K/h. This procedure is also referred to as furnace cooled (fc). In order to realize different cooling rates, the glass NBS2 was additionally poured into graphite molds preheated and subsequently annealed from various temperatures. The temperature of those preheated graphite molds is referred to as melt cooling temperature T_{mc} ranging from RT to 750°C. The largest cooling rate was realized by rapidly quenching the melt to RT by pressing between two copper blocks. This state is also referred to as quenched (qu).

Commercial vitreous SiO_2 was studied for comparison of a fully polymerized glass. More details on melting procedures and additional information on the structural as well as mechanical studies of the NBS glasses can be found in the literature (Winterstein-Beckmann et al., 2014; Malchow et al., 2015; Möncke et al., 2003, 2006, 2015a).

General Glass Characterization

The glass density ρ was measured by the Archimedes method with dry ethanol as immersion liquid. Differential scanning calorimetry was used to determine the glass transition temperature T_g on powdered glass samples with a heating rates of 10 K/min, taking the onset. The coefficient of thermal expansion was determined by dilatometry with a heating rate of 10 K/min for the borosilicate

glasses, and a heating rate of 5 K/min for borate glasses on 11 mm long glass cylinders.

As-cast glass samples were cut with a diamond saw such that indented surfaces corresponded to the center of the cast. Surfaces were mechanically ground with *SiC* grinding paper and ethanol based lubrication followed by polishing with 3 and 1 μm diamond particles in declining order.

In addition to the more detailed mechanical testing described in Sections "Nanoindentation Testing" and "Nano-Impact Testing," the mechanical properties of the studied glasses had been routinely determined by ultrasonic echography and nanoindentation. Elastic properties can be derived from ultrasonic echography which records the sound wave propagation times. An echometer (model 1077, Karl Deutsch GmbH) working with an accuracy of ±1 ns was employed. More information on ultrasonic measurements and how elastic properties such as shear modulus G, bulk modulus K, and Young's modulus E, and Poisson ratio ν can be found elsewhere (Limbach et al. 2015; Möncke et al., 2016).

Nanoindentation Testing

Instrumented indentation testing using a Keysight Nano Indenter® G200 (Keysight Technologies, Inc., Santa Rosa, CA, USA) was performed at room temperature under ambient pressure with three-sided diamond Synton (Synton-MDP AG, Nidau, Switzerland) Berkovich and Cubecorner tips having a nominal centerline-to-face angle of 65.27° and 35.26°, respectively. Machine compliance and tip area function were calibrated using a fused silica reference sample according to the method suggested by Oliver and Pharr. Maximum indentation depth was 2,000 nm with a peak-load hold time of 5 s (Oliver and Pharr, 1992, 2004).

Elastic modulus E and hardness H were estimated using the continuous stiffness measurement (CSM) method, where the unloading stiffness S is measured as a function of depth. A harmonic displacement oscillation of 2 nm and an indentation strain rate of 0.05 s^{-1} were used. Hardness and elastic modulus results were averaged over a displacement range of 1,000–2,000 nm and averaged again over all nine performed CSM indentations. In contrast, a nanoindentation strain rate jump test was applied to determine the values of m as well as the activated volume V. The tests were performed using strain rates of 0.05, 0.007, and 0.001 s^{-1}. The displacement per rate amounted to 300 nm. More details can be found elsewhere (Maier et al., 2011).

The onset of cracking was studied using a load controlled (LC) method, where the load was applied linearly with a rate of 10 gf/s, and the peak-load hold time amounted to 10 s. Nine indentations were performed each, aligned in a 3 × 3 Matrix.

Nano-Impact Testing

A Micro Materials Ltd. Platform 3 nanoindenter was used to investigate the effect of multiple impact indentation on NBS2 samples. A multiple impulse test method was used. This method uses a pendulum-based nanoindentation setup, where the pendulum is stressed by applying voltage to a solenoid on both ends of the pendulum (**Figure 1A**). The top solenoid has a fixed position and maintains a variable load (pre load) on the pendulum throughout the whole experiment. By varying this pre load, the maximum velocity of the indenter during the first impact can be controlled. The position of the bottom solenoid is not fixed, which allows an initial impact height to be set, changing for example the distance between the sample and indenter in the initial, stressed position. Upon releasing the pendulum from the bottom solenoid, it accelerates with a high force and swings toward the sample, resulting in an impact of the indenter tip on the sample with a high velocity (**Figure 1B**). The velocity of the indenter will decrease during the indentation process until the complete kinetic energy is absorbed by the material and the indenter comes to rest at the maximum indentation depth. The high amount of elastic deformation leads to a backward movement and even a springback and a following second indentation process of the indenter. This process repeats several times till all kinetic energy is transformed into plastic deformation.

The load applied by the top solenoid was altered throughout the experiment. Forces of 1, 5, 10, 20, 50, and 100 mN were used. The impact height was maintained at 5,000 nm throughout the experiment. The tested samples were quenched to room temperature (quenched) and slowly cooled from 700°C (furnace cooled). Both were melted at 1,650°C.

The position of the indenter tip, in relation to the sample surface, was recorded for 0.5 s at 8,000 Hz upon releasing the pendulum. Then, the pendulum was retracted again by switching on the bottom solenoid. This process was repeated multiple times at the same location, thus delivering multiple impact tests. One hundred forty impacts per site were conducted with loads of 1, 5, 10, and 20 mN. Fifty and 10 impacts were conducted with 50 and 100 mN, respectively. This set of tests was conducted for both samples. In addition to this, 5, 50, 100, and 150 impact-indents per site were made on the furnace cooled (fc) with 20 mN, as well as 10 and 20 impact per site with 50 mN.

RESULTS AND DISCUSSION

Mechanical Testing of NBS2 Glasses with Different Network Connections

Section "Introduction" summarized some detailed structural information regarding the effect of processing on the connectivity of borate and silicate entities in the low-alkaline borosilicate glass NBS2. In the following sections, new data on the mechanical response of such differently processed NBS2 glass samples are presented and set in comparison with earlier results. We did not only compare quenched and annealed glasses but also looked at glasses prepared at different melting temperatures (from 1,650 to 1,750°C) and glasses annealed from the melt at different cooling temperatures. A higher melting temperature and lower annealing temperature result in a faster cooling rate and thus less time for borate and silicate entities to find their preferred bonding partners. Therefore, the fast quenched glass shows the highest number of mixed bonds; glasses annealed above T_g (440°C) have the highest number of homopolar B-O-B and Si-O-Si bonds. To further investigate the effect of high cooling rates, two quenching modes were utilized: T_{mc} = RT means that the melt was only poured onto a brass block and allowed to cool, which for a 5- to 8-mm thick sample will take a while. Conversely, the term "quenched" described samples that were splat quenched between

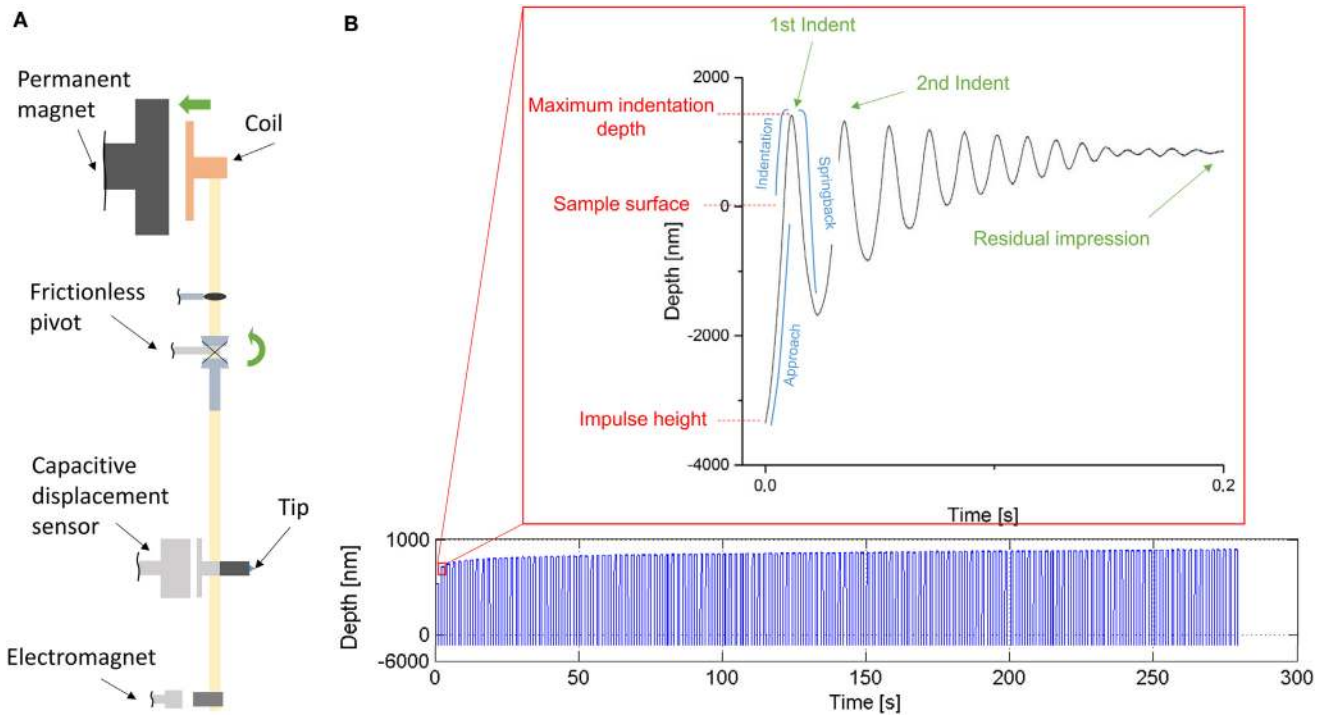

FIGURE 1 | Schematic scetch of the pendulum-based nanoindenter NanoTest Platform III for impact testing (A) and a typical depth-time signal obtained during impact testing (B). The Inset in **(B)** displays the high-resolution signal during one impact.

two brass blocks, a technique by which the heat dissipates faster and the melt is flatted to a thickness of only ca. 3 mm, resulting in a very high cooling rate.

Figures 2A,B show how the Young's modulus E and hardness H vary with increasing melt cooling temperature T_{mc}, e.g., decreasing cooling rate. The mechanical response was calculated using the Oliver–Pharr technique as presented in Section "Mechanical Testing of Glass." The effect of processing parameters on Young's modulus and hardness is negligible. E fluctuates with a standard deviation σ of 0.96 GPa around an average value of $E = 52.35$ GPa, while the average H amounts to 6.45 GPa with $\sigma = 0.17$ GPa. The same can be observed for the indentation parameter S^2/P. As before, no influence of the processing conditions can be found. The average value amounts to 535.31 GPa with $\sigma = 12.86$ GPa. The standard deviation is highlighted as light gray area in **Figure 2**, whereas the average value is represented as a dotted line. The viscosity of the NBS2 glass at 1,650°C is observable higher than at 1,700°C or 1,750°C, which might account for larger scattering of data in the series melted at 1,650°C. The values of the E and H plotted in **Figure 2** vary by only 5%, which is within the experimental error margins and very close to the ultrasonic determined Young's modulus of 55.7 GPa. Therefore, no significant difference in E or H can be pronounced from the apparent slight increase of E and H data by this method alone.

Strain Rate Sensitivity

Strain rate jump test results for NBS2 glass with various cooling paths coming from $T_m = 1{,}750$°C are shown in **Figure 3**. Loading started with an initial strain rate of 0.05 s^{-1}. The fist strain rate jump to 0.007 s^{-1} was performed at an indentation depth of 700 nm and, with a drop of 5%, triggered a clear variation in the hardness course. Hardness was averaged after it settled on an even plateau in the final 200 nm displacement per strain rate jump. The second jump from 0.05 s^{-1} down to 0.001 s^{-1} was performed at an indentation depth of 1,300 nm resulting in a 9% drop of hardness.

A strain rate sensitivity was observed for various processing conditions including different melting and annealing temperatures as well as for quenched NBS2 glasses. **Figure 4A** shows the strain rate sensitivity m, calculated according to Eq. 4, for the strain rate jump from 0.05 s^{-1} to 0.007 s^{-1} as a function of the processing conditions of the NBS2 glass. Taking into account the measurement uncertainty, an effect of the processing conditions is negligible. The mean value of coefficient m amounts to 0.0231. The corresponding activation volume V shows negligible influence of the processing conditions as well. The average amounts to 0.0713 nm^3 for the NBS2 glass. The results are summarized in **Table 1**.

Onset and Types of Cracking

The onset of cracking was studied with LC indentations with a Berkovich indenter, where the load was increased in steps of 100 gf or 0.98 N, respectively. The probability for radial cracking was calculated referring the number of indent edges that contain cracks to the total number of indent edges. Although **Figure 5** only considers radial cracks, different crack types were observed as well. Actually in most cases, radial cracking occurred

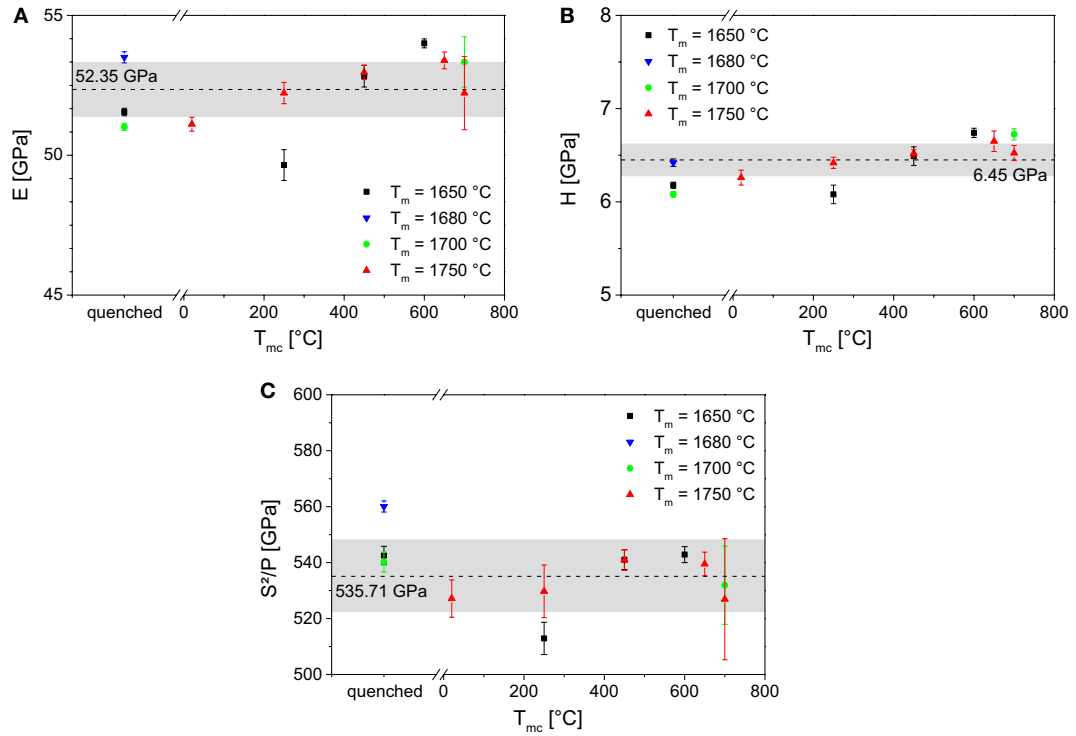

FIGURE 2 | **(A)** Young's modulus, **(B)** hardness, and **(C)** S^2/P as a function of the processing parameters. For each parameter, the average value is plotted as a dashed line and its SD as light gray area.

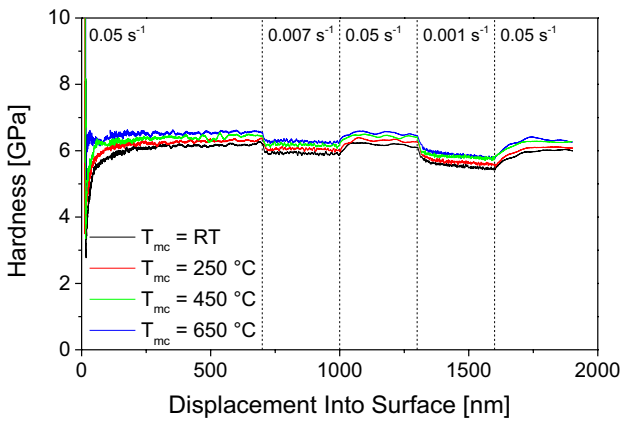

FIGURE 3 | **Changes in hardness caused by with strain rate jumps in NBS2 glass with various melt cooling temperature T_{mc} (T_m = 1,750°C).**

combined with other types, e.g., chipping or conical cracking. A generic crack development is visualized in the laser scanning micrographs of **Figure 6**. For all indentation loads, the indent surface exhibits shear artifacts at the contact areas (**Figure 6A**). It is difficult to identify whether those artifacts are real cracks or if they result only from laser interference. For the given processing condition, cracking starts with the development of radial cracks at 500 gf. However, in many cases, chipping was observed as well. Increasing the indentation load induces cone cracking, which connects the contact edges, additional to the radial cracks (**Figure 6C**). However, total destruction could also be observed at similar indentation loads (**Figure 6D**).

Nano-Impact Testing

The dynamic cracking behavior was characterized using the nano-impact testing technique. **Figure 7** shows the depth–time curves for the two samples tested with 20 mN up to 140 times on the same site. There are clear differences in the behavior of the quenched and the furnace cooled sample. The most obvious difference is the amount of cracking. Although cracking is not observed in the quenched sample after 140 cycles with 20 mN, a large amount of cone and lateral cracks are seen in the furnace cooled sample after 140 cycles. This result is reproducible at 50 and 100 mN. In both instances the furnace cooled sample offers chipping already after a few cycles, while the quenched sample does not show cracking even after 50 cycles at 50 mN and 10 cycles at 100 mN. For loads lower than 20 mN, cracking could not be initiated in either sample within the 140 cycles tested.

Furthermore, differences in the shape of the depth–time curves are clearly apparent. For samples in which cracking occurs, there is a sudden increase in depth, marking the point of crack initiation. This sudden increase in depth appears in all measurements where cracking is observed, but is absent in those measurements where no cracking occurs. **Figure 7A** shows this feature at 105 cycles (200 s). Several tests have been conducted at 20 mN with

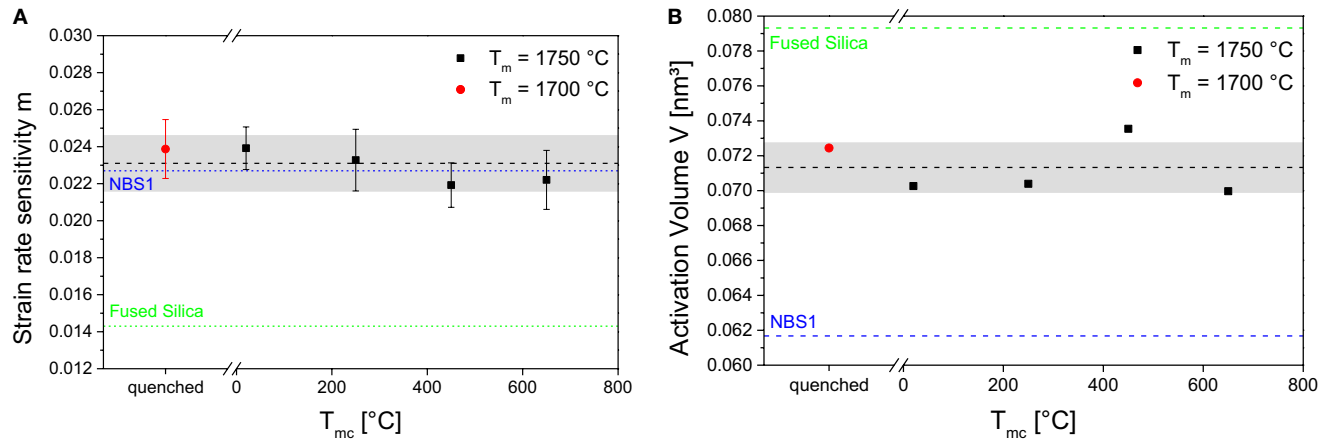

FIGURE 4 | **(A)** Coefficient of strain rate sensitivity *m* and **(B)** the activation volume *V* as a function of processing conditions in NBS2 glass. Fused silica (green) and NBS1 (blue) are plotted as comparison.

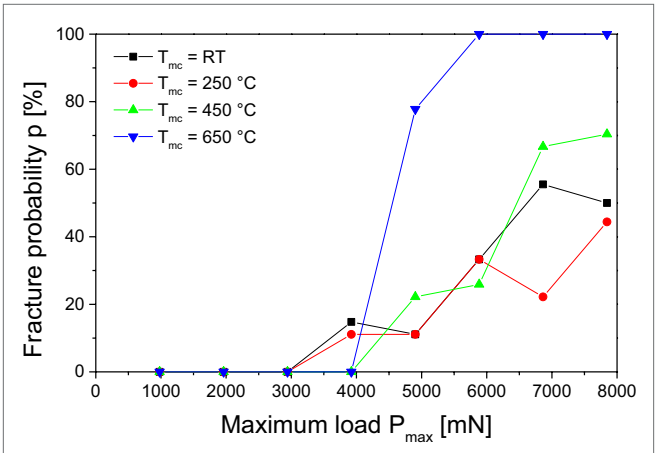

FIGURE 5 | **The probability for radial cracking as a function of the indenter load during Berkovich indentation for several processing conditions (T_m = 1,750°C)**.

1, 50, and 100 impacts to visualize the onset of cracking. After 100 cycles, one can see a pileup at the edge of the indent (**Figure 7A** inset at 100×). However, it is also apparent that no complete crack has formed yet. The critical number of cycles required to initiate cracking in the furnace cooled sample decreases with increasing load from 37 at 10 mN to 21 at 20 mN, 7 at 50 nN, and 2 at 100 mN, respectively.

DISCUSSION

Mechanical Properties of NBS2 Glasses with Different Network Connectivities

The results presented in **Figure 2** show that the processing conditions have minor influence on the mechanical response of the NBS2 glass in terms of *H* and *E*. The SDs for Young's modulus, hardness, and the S^2/P parameter are with less than 3% quite small and give a reproducible impression of the mechanical response of the NBS2 glasses. Young's modulus corresponds very well with the data presented in former studies (Malchow et al., 2015). However, Malchow et al. determined lower hardness values for the furnace cooled glass compared to quenched ones, so we expected a decreasing hardness with increasing annealing temperature. In contrast, our results indicate a constant hardness level almost uninfluenced by processing conditions.

The onset of cracking is of key interest when it comes to the application of glasses. Malchow et al. (2015) compared the crack probability of quenched and furnace cooled NBS2 samples during quasi-static indentation. In the furnace cooled condition, the onset of cracking was observed at lower loads compared to the quenched samples. This means that an increasing cooling rate improves the crack resistance behavior. This is correlated to a larger amount of densification in the quenched sample compared to the furnace cooled one (Bruns et al., 2017). The crack probability study in this study (**Figure 5**) focuses on intermediate processing conditions, corresponding to a variation of the melt cooling temperature T_{mc}. Samples with T_{mc} between RT and 450°C show similar cracking probability, and the observable deviation is rather an effect of scattering than a real influence of the processing conditions. It is interesting to note that the upper limit of 450°C is close to the T_g of NBS2, which is 440°C. The samples exhibit a crack probability field, i.e., for loads inside this probability field, some indents showed cracking, whereas others did not. In contrast, the furnace cooled condition (T_{mc} = 650°C) did not show this kind of behavior. Once cracking started, all indents were damaged, consistent with former studies (Malchow et al., 2015). These results indicate that cooling rates as high as quenching are not necessarily required to improve the crack resistance. As long as T_g is passed with a relative high cooling rate, a structure is created, which hinders cracking effectively. A further increase in cooling rates does not show an improvement in crack resistance.

Evaluation of fracture toughness following the approach of Lawn et al. (1980) requires accurate determination of radial crack lengths. Even though the development of radial cracks

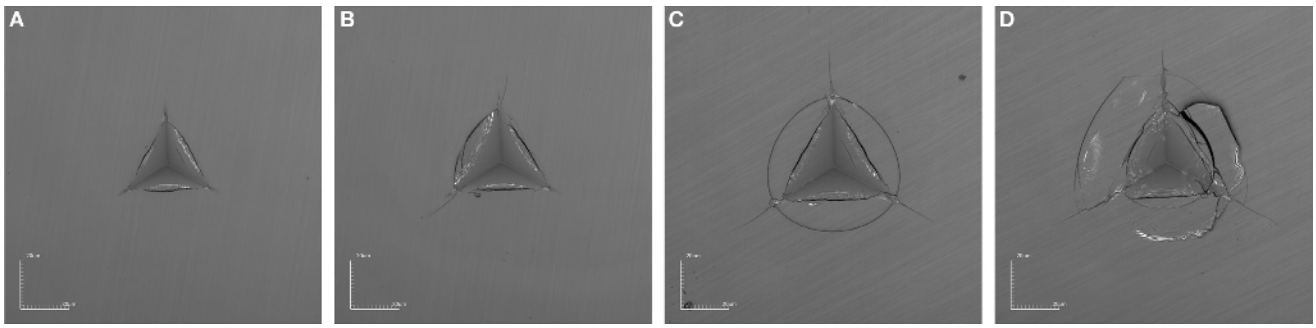

FIGURE 6 | Crack development during Berkovich indentation in NBS2 glass (T_m = 1,750°C and T_{mc} = 450°C) at (A) 400 gf, (B) 500 gf, and (C) as well as (D) at 700 gf taken with a laser scanning microscope.

was observed during Berkovich indentation testing, it was not possible to generate such cracks in a reproducible manner to perform fracture toughness treatments. Also in the intermediate loading regime, radial cracking occurred almost always in combination with other types of cracks. In the few cases that show exclusively radial cracking, the path of the cracks often deviates from perfect alignment as extension of the indenter edge as can be seen in **Figure 6B**. Both influences the radial extension and makes fracture toughness analysis using the approach of Lawn et al. difficult.

The Effect of Strain Rate on the Deformation Mechanism

The effect of strain rate on the deformation mechanisms in glasses with different structures was investigated. Strain rate sensitivity measurements performed on various processing conditions show that NBS2 glass indeed exhibits strain rate-dependent hardness values (**Figure 3**). As observed for E, S^2/P, and H, neither the coefficient of strain rate sensitivity m nor the activated volume V are influenced by the variation of processing conditions performed in this study (**Figure 4**). For comparison, a strain rate study was performed on fused silica and the NBS1 borosilicate as well, and strain rate sensitivity was observed for both, too (**Table 1**). Strain rate sensitivity has been reported for both types of glasses, normal and anomalous glasses. Limbach et al. (2014) found a strong strain rate sensitivity for glasses with intermediate Poisson's ratios. For low (strongly cross-linked glasses) and high (planar structures with limited cross-linking between the single planes) values, low strain rate sensitivity was found. Different other authors report strain rate sensitivity during creep indentation tests when glasses are tested in water, which is known to affect the glass structure (Han and Tomozawa, 1990; Keulen, 1993; Shang and Rouxel, 2005). This effect can also be seen in our study. At a value of 0.023, m is almost the same for both borosilicate glasses, NBS1 and NBS2. Both glasses exhibit a Poisson ratio of 0.21. Fused Silica in turn offers with 0.014, a much smaller coefficient m; this is accompanied by a lower Poisson's ratio of 0.18 (Han and Tomozawa, 1990; Keulen, 1993; Shang and Rouxel, 2005).

However, the activation volume has not been considered in the studies on silicate glasses. We found that fused silica exhibits the largest value, followed by NBS2 and NBS1 in a declining order. Interestingly the amount of densification within the glass decreases in the same sequence. According to the density of the individual glasses (**Table 1**), the activation volume contains five, five, and four atoms with an average atomic mass M for fused silica, NBS2, and NBS1, respectively.

$$M = \left(\sum_i^n \mathrm{A}_i \mathrm{m}_i^3 \right)^{\frac{1}{3}}, \tag{6}$$

where A_i is the atomic fraction and m_i the atomic mass of each element.

The number of atoms thermally activated by changes in strain rate is small for all examined glasses. The low number indicates that deformation in (boro-) silicate glasses is rather an individual atom motion than cooperative shearing of unstable clusters as observed in shear transformation zones in bulk metallic glasses (Pan et al., 2008). However, so far it is unclear whether individual structural units, the network connectivity, or the free volume itself is responsible for strain rate sensitivity.

In general, both processes, densification and shear flow are sensitive toward changes in strain rate (Shikimaka et al., 2016); the contribution of each, however, depends on composition, atomic packing density, and network connectivity (Yoshida et al., 2005; Limbach et al., 2014; Möncke et al., 2016). Shikimaka et al. (2016) concluded densification to be triggered by shear and pressure. This is supported by Mackenzie, who argues that densification is basically an entanglement of structural units. This would mean that the main part of densification takes place during shear deformation (Mackenzie, 1963). Thus, an increasing activation of shear deformation (Limbach et al., 2014) would be transferred to an increasing amount of densification. Performing post indent annealing experiments, Shikimaka et al. have shown that densification contribution to plastic flow is larger for small strain rates. At small strain rates, the material behaves softer and rearrangement processes in the material become easier (Shikimaka et al., 2016). That is why lower strain rates result in lower hardness values, which agrees very well with our results (**Figure 3**).

If densification improves the crack resistance (Malchow et al., 2015) and is more pronounced at small strain rates, it raises the

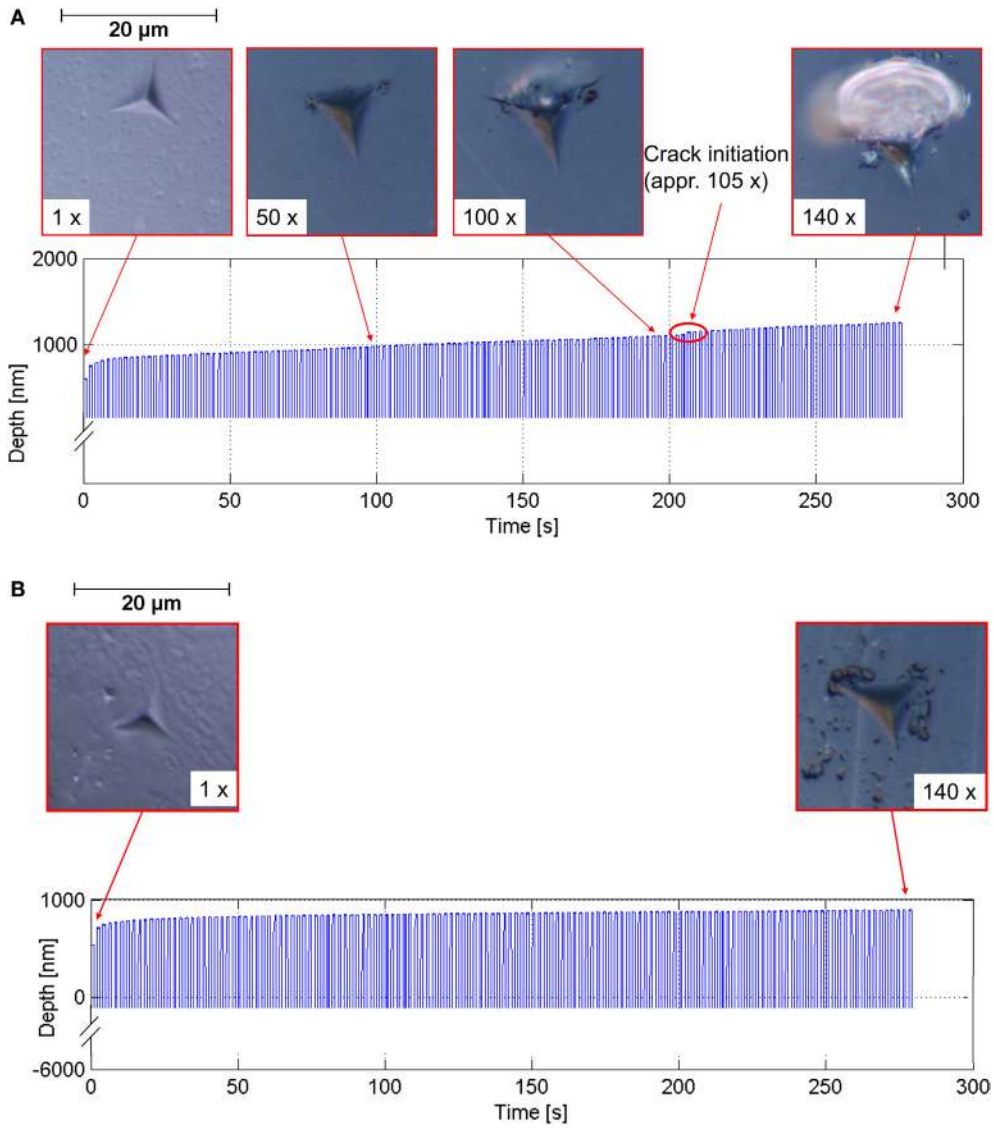

FIGURE 7 | Depth–time curve of multiple impulse tests on a NBS2 (T_m = 1,650°C) furnace cooled [(A), T_{mc} = 700°C] and quenched (B) sample with 20 mN up to 140 times on the same site. Insets show the indent after different number of tests.

question how cracking is influenced by changes in strain rate. Nano-impact testing causes strain rates 3–5 orders of magnitude larger than conventional indentation testing, hence in a range dominated by shear flow. In this study, only the two extreme cases, NBS2 glass with the smallest (furnace cooled) and the largest cooling rate (quenched) from 1,650°C, were considered. Quasi-static indentation revealed the furnace cooled processing condition to offer the poorest cracking resistance. A similar behavior is observable for impact indentation testing. Although quenched NBS2 repelled crack initiation even after 10 cycles with 100 mN pre load, furnace cooled NBS2 started cracking already after four impact cycles. This behavior was reproducible for pre loads of 50 and 20 mN, the extreme being 50 mN. Comparing the performance of both glasses at this level visualizes a remarkable improvement of the cracking resistance. While furnace cooled NBS2 started cracking after seven cycles, quenched NBS2 resisted cracking for even 50 cycles. This would indicate a seven times larger cracking resistance for the quenched NBS2 glass. However, it should be mentioned that quenched glasses exhibit more strain than carefully furnace cooled glass samples, and the data of any measured property scatter more for quenched samples.

These results confirm the previous discussed view on strain rate sensitivity in glasses: though both mechanisms, densification and shear deformation, show strain rate sensitivity, shear deformation becomes more and more important for higher strain rate. The higher cracking resistance for the quenched glass is related to the higher amount of densification in this glass (Malchow et al., 2015). This effect is even more pronounced at high strain rates. It

indicates that the furnace cooled glass, which is known to deform to a larger extend by shear processes, shows a stronger dependency of cracking probability on the strain rate than the quenched glass. The application of this new method to different glasses will help setting these results in comparison to other systems.

The second finding revealed that no transitional zone in the furnace cooled glass for impact loading could be detected within the accuracy of this experiment. This is contrary to most glasses, in which a load-range exists in which cracking occurs with a certain probability. Instead, the furnace cooled NBS2 samples show either cracking or no cracking during quasi-static testing. In impact testing, distinct steps in the otherwise steady and linear increasing depth–time curves are evident in **Figure 7**. We could establish that these steps are connected to the onset of cracking, as they only appear in indents in which posttest cracks can be observed as well. This demonstrates that cracking occurs spontaneously, i.e., without crossing a probability range at certain loading conditions, as it was already found for the furnace cooled glass under quasi-static loading. **Figure 8** displays the critical load to initiate cracking with a certain number of cycles. Here, it is obvious that once cracks can be initiated, the critical load increases rapidly. This illustrates that the transitional zone is indeed very narrow as was already discussed for quasi-static indentation (**Figure 5**) or at least that the transition range is very narrow for the furnace cooled sample (Malchow et al., 2015).

CONCLUSION

The low-alkali borosilicate glass NBS2 is known to exhibit anomalous, i.e., densification-driven, rather than shear driven, deformation behavior. It has been shown previously that the connectivity of borate and silicate entities in the NBS2 glass vary significantly with thermal history during processing, that is, with the final melting temperature and the cooling rate.

For fast cooling rates, the extreme being the quenched glasses, the high disorder from the melt is frozen. This results in a more random connectivity between borate and silicate units. A higher number of mixed Si-O-B bonds is found, and BO_3 triangles are inserted into the three-dimensional silicate network instead of forming planar three-membered boroxol rings. Such a network is expected to exhibit a larger free volume compared to the preferential network in slowly cooled, annealed NBS2 glasses with a higher fraction of Si-O-Si and B-O-B bonds, arranged in the typical silicate and borate rings. As a result, the glass structure becomes more open. A more open structure in turn increases the potential for densification. In this manner, quenched NBS2 offers a larger ability for densification compared to furnace cooled one (Malchow et al., 2015). However, neither E, H, and m seem to change for different cooling rates. The amount of energy dissipated by densification reduces the amount of shear taking place, which reduces the probability for cracking as a smaller amount of residual stresses is introduced and maintained in the deformed volume (Kato et al., 2010; Gross, 2012; Sellappan et al., 2013; Bruns et al., 2017). This correlation is observed for impact and quasi-static indentation testing, both showing a larger threshold load for the activation of cracks for samples that were quenched than for annealed ones. The parameter controlling the cracking resistance is shown to be the cooling rate at T_g. Once T_g was crossed with a relative high cooling rate, crack initiation was shifted drastically to higher loads. Further increase in cooling rate did not show a change in crack resistance. As the borosilicate was found to be strain rate sensitive, the onset of cracking was even more shifted applying larger strain rates by nano-impact testing. Since shear flow, which is known to be more sensitive to changes in strain rate, is the dominating process in the closer packed furnace cooled glass, it appears obvious that the crack probability distribution diverges more in the dynamic case.

The strain rate sensitivity of NBS2 was compared with the highly densifyable fused silica and the normal behaving NBS1 borosilicate. It has been noticed that the activation volume increases in the same order as the densification ability of the glasses. A correlation to the glass topology, however, requires further investigation.

These findings offer important insights for the design process of crack-resistant borosilicate glasses. Especially for applications where high strain rates are possible, crossing T_g with high quenching rates will result in a larger amount of shear deformation and less cracking.

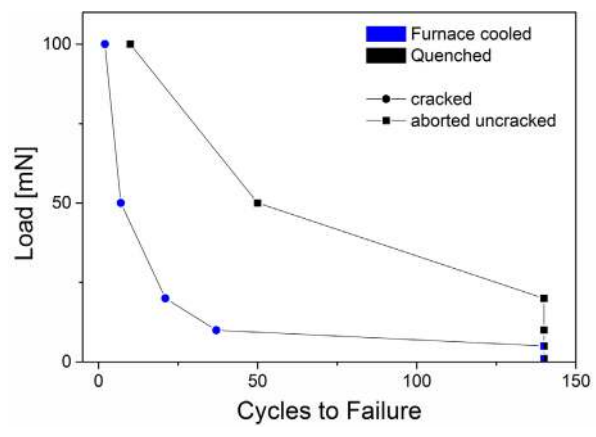

FIGURE 8 | The critical cycle number for crack initiation for different loads for the furnace cooled and the quenched sample.

AUTHOR CONTRIBUTIONS

KD, SK-K, and DM are responsible for the concept and design of this project within the priority program. Data acquisition and interpretation were realized by all co-authors as well as by several co-workers, who contributed earlier to the work of the cited references. Acquisition, analysis, and evaluation of the new data presented in this study was primarily realized by SB (static indentation), CZ, and J-NP (nano-impact testing). All authors contributed through the writing of different sections and through critical contributions to the rest of the manuscript, including revision and all authors approved the final version.

ACKNOWLEDGMENTS

Fruitful discussions with Lothar Wondraczek and Sindy Fuhrmann (OSIM, Jena) are gratefully acknowledged. We also want to express our thanks to Efstratios I. Kamitsos and Dimitrios Palles (NHRF, Athens) for helpful discussion.

FUNDING

The authors are grateful for financial support from the German Science Foundation through its priority program SPP 1594 and the German-Greek program IKYDA 2015 for the promotion of exchange and scientific cooperation between Greece and Germany.

REFERENCES

Arora, A., Marshall, D. B., and Lawn, B. R. (1979). Indentation deformation/fracture of normal and anomalous glasses. *J. Non Cryst. Solids* 31, 415–428. doi:10.1016/0022-3093(79)90154-6

Barlet, M., Delaye, J.-M., Charpentier, T., Gennisson, M., Bonamy, D., Rouxel, T., et al. (2015). Hardness and toughness of sodium borosilicate glasses via Vickers's indentations. *J. Non Cryst. Solids* 417–418, 66–79. doi:10.1016/j.jnoncrysol.2015.02.005

Beake, B. D., Fox-Rabinovich, G. S., Veldhuis, S. C., and Goodes, S. R. (2009). Coating optimisation for high speed machining with advanced nanomechanical test methods. *Surf. Coat. Technol.* 203, 1919–1925. doi:10.1016/j.surfcoat.2009.01.025

Beake, B. D., García, M. A. J. I., and Smith, J. F. (2001). Micro-impact testing: a new technique for investigating fracture toughness. *Thin Solid Films* 398–399, 438–443. doi:10.1016/S0040-6090(01)01397-9

Beake, B. D., and Smith, J. F. (2004). Nano-impact testing—an effective tool for assessing the resistance of advanced wear-resistant coatings to fatigue failure and delamination. *Surf. Coat. Technol.* 188–189, 594–598. doi:10.1016/j.surfcoat.2004.07.016

Brawer, S. A., and White, W. B. (1975). Raman spectroscopic investigation of the structure of silicate glasses. I. The binary alkali silicates. *J. Chem. Phys.* 63, 2421–2432. doi:10.1063/1.431671

Bruns, S., Johanns, K. E., Rehman, H. U. R., Pharr, G. M., and Durst, K. (2017). Constitutive modeling of indentation cracking in fused silica. *J. Am. Ceram. Soc.* doi:10.1111/jace.14734

Durst, K., and Maier, V. (2015). Dynamic nanoindentation testing for studying thermally activated processes from single to nanocrystalline metals. *Curr. Opin. Solid State Mater. Sci.* 19, 340–353. doi:10.1016/j.cossms.2015.02.001

Gross, T. M. (2012). Deformation and cracking behavior of glasses indented with diamond tips of various sharpness. *J. Non Cryst. Solids* 358, 3445–3452. doi:10.1016/j.jnoncrysol.2012.01.052

Guerette, M., Ackerson, M. R., Thomas, J., Yuan, F., Bruce Watson, E., Walker, D., et al. (2015). Structure and properties of silica glass densified in cold compression and hot compression. *Sci. Rep.* 5, 15343. doi:10.1038/srep15343

Han, W.-T., and Tomozawa, M. (1990). Indentation creep of Na2O 3SiO2 glasses with various water contents. *J. Am. Ceram. Soc.* 73, 3626–3632. doi:10.1111/j.1151-2916.1990.tb04268.x

Jennett, N. M., and Nunn, J. (2011). High resolution measurement of dynamic (nano) indentation impact energy: a step towards the determination of indentation fracture resistance. *Philos. Mag.* 91, 1200–1220. doi:10.1080/14786435.2010.485585

Joslin, D. L., and Oliver, W. C. (1990). A new method for analyzing data from continuous depth-sensing microindentation tests. *J. Mater. Res.* 5, 123–126. doi:10.1557/Jmr.1990.0123

Kato, Y., Yamazaki, H., Kubo, Y., Yoshida, S., Matsuoka, J., and Akai, T. (2010). Effect of B2O3 content on crack initiation under Vickers indentation test. *J. Ceram. Soc. Jpn.* 118, 792–798. doi:10.2109/jcersj2.118.792

Keulen, N. M. (1993). Indentation creep of hydrated soda–lime silicate glass determined by nanoindentation. *J. Am. Ceram. Soc.* 76, 904–912. doi:10.1111/j.1151-2916.1993.tb05314.x

Lawn, B. R., Evans, A. G., and Marshall, D. B. (1980). Elastic/plastic indentation damage in ceramics: the median/radial crack system. *J. Am. Ceram. Soc.* 63, 574–581. doi:10.1111/j.1151-2916.1980.tb10768.x

Lee, S. K., Eng, P. J., Mao, H.-K., Meng, Y., Newville, M., Hu, M. Y., et al. (2005). Probing of bonding changes in B2O3 glasses at high pressure with inelastic X-ray scattering. *Nat. Mater.* 4, 851–854. doi:10.1038/nmat1511

Limbach, R., Rodrigues, B. P., and Wondraczek, L. (2014). Strain-rate sensitivity of glasses. *J. Non Cryst. Solids* 404, 124–134. doi:10.1016/j.jnoncrysol.2014.08.023

Limbach, R., Winterstein-Beckmann, A., Dellith, J., Möncke, D., and Wondraczek, L. (2015). Plasticity, crack initiation and defect resistance in alkali-borosilicate glasses: from normal to anomalous behavior. *J. Non Cryst. Solids* 417-418, 15–27. doi:10.1016/j.jnoncrysol.2015.02.019

Mackenzie, J. D. (1963). High-pressure effects on oxide glasses: I, densification in rigid state. *J. Am. Ceram. Soc.* 46, 461–470. doi:10.1111/j.1151-2916.1963.tb13776.x

Maier, V., Durst, K., Mueller, J., Backes, B., Höppel, H. W., and Göken, M. (2011). Nanoindentation strain-rate jump tests for determining the local strain-rate sensitivity in nanocrystalline Ni and ultrafine-grained Al. *J. Mater. Res.* 26, 1421–1430. doi:10.1557/jmr.2011.156

Malchow, P., Johanns, K. E., Möncke, D., Korte-Kerzel, S., Wondraczek, L., and Durst, K. (2015). Composition and cooling-rate dependence of plastic deformation, densification, and cracking in sodium borosilicate glasses during pyramidal indentation. *J. Non Cryst. Solids* 419, 97–109. doi:10.1016/j.jnoncrysol.2015.03.020

Mayo, M. J., and Nix, W. D. (1988). A micro-indentation study of superplasticity in Pb, Sn, and Sn-38 wt% Pb. *Acta Metall.* 36, 2183–2192. doi:10.1016/0001-6160(88)90319-7

Möncke, D., Dussauze, M., Kamitsos, E. I., Varsamis, C. P. E., and Ehrt, D. (2009). Thermal poling induced structural changes in sodium borosilicate glasses. *Phys. Chem. Glasses Eur. J. Glass Sci. Technol. Part B* 50, 229–235.

Möncke, D., and Ehrt, D. (2002). Influence of melting and annealing conditions on the optical spectra of a borosilicate glass doped with CoO and NiO. *Glass Sci. Technol.* 75, 163–173.

Möncke, D., Ehrt, D., Eckert, H., and Mertens, V. (2003). Influence of melting and annealing conditions on the structure of borosilicate glasses. *Phys. Chem. Glasses* 44, 113–116.

Möncke, D., Ehrt, D., and Kamitsos, E. I. (2013). Spectroscopic study of manganese-containing borate and borosilicate glasses: cluster formation and phase separation. *Phys. Chem. Glasses Eur. J. Glass. Sci. Technol. Part B* 54, 42–51.

Möncke, D., Ehrt, D., Varsamis, C.-P. E., Kamitsos, E. I., and Kalampounias, A. G. (2006). Thermal history of a low alkali borosilicate glass probed by infrared and Raman spectroscopy. *Glass Technol. Eur. J. Glass Sci. Technol. Part A* 47, 133–137.

Möncke, D., Kamitsos, E. I., Palles, D., Limbach, R., Winterstein-Beckmann, A., Honma, T., et al. (2016). Transition and post-transition metal ions in borate glasses: borate ligand speciation, cluster formation, and their effect on glass transition and mechanical properties. *J. Chem. Phys.* 145, 124501. doi:10.1063/1.4962323

Möncke, D., Tricot, G., Ehrt, D., and Kamitsos, E. I. (2015a). Connectivity of borate and silicate groups in a low-alkali borosilicate glass by vibrational and 2D NMR spectroscopy. *J. Chem. Technol. Metall.* 50, 381–386.

Möncke, D., Tricot, G., Winterstein-Beckmann, A., Wondraczek, L., and Kamitsos, E. I. (2015b). On the connectivity of borate tetrahedra in borate and borosilicate glasses. *Phys. Chem. Glasses* 56(5), 203–211. doi:10.13036/17533562.56.5.203

Morozumi, H., Yoshida, S., and Matsuoka, J. (2016). Composition dependence of crack formation probability in aluminoborosilicate glass. *J. Non Cryst. Solids* 444, 31–37. doi:10.1016/j.jnoncrysol.2016.04.030

Oliver, W. C., and Pharr, G. M. (1992). An improved technique for determining hardness and elastic modulus using load and displacement sensing indentation experiments. *J. Mater. Res.* 7, 1564–1583. doi:10.1557/JMR.1992.1564

Oliver, W. C., and Pharr, G. M. (2004). Measurement of hardness and elastic modulus by instrumented indentation: advances in understanding and refinements to methodology. *J. Mater. Res.* 19, 3–20. doi:10.1557/jmr.2004.0002

Pan, D., Inoue, A., Sakurai, T., and Chen, M. W. (2008). Experimental characterization of shear transformation zones for plastic flow of bulk metallic glasses. *Proc. Natl. Acad. Sci. U.S.A.* 105, 14769–14772. doi:10.1073/pnas.0806051105

Rouxel, T., Ji, H., Guin, J. P., Augereau, F., and Rufflé, B. (2010). Indentation deformation mechanism in glass: densification versus shear flow. *J. Appl. Phys.* 107, 094903. doi:10.1063/1.3407559

Rouxel, T., Sellappan, P., Celarie, F., Houizot, P., and Sangleboeuf, J. C. (2014). Toward glasses with better indentation cracking resistance. *Comptes Rendus Mecanique* 342, 46–51. doi:10.1016/j.crme.2013.10.008

Sellappan, P., Rouxel, T., Celarie, F., Becker, E., Houizot, P., and Conradt, R. (2013). Composition dependence of indentation deformation and indentation cracking in glass. *Acta Mater.* 61, 5949–5965. doi:10.1016/j.actamat.2013.06.034

Shang, H., and Rouxel, T. (2005). Creep behavior of soda-lime glass in the 100–500 K temperature range by indentation creep test. *J. Am. Ceram. Soc.* 88, 2625–2628. doi:10.1111/j.1551-2916.2005.00464.x

Shikimaka, O., Grabco, D., Sava, B. A., Elisa, M., Boroica, L., Harea, E., et al. (2016). Densification contribution as a function of strain rate under indentation of terbium-doped aluminophosphate glass. *J. Sci. Mater.* 51, 1409–1417. doi:10.1007/s10853-015-9460-8

Somekawa, H., and Schuh, C. A. (2012). High-strain-rate nanoindentation behavior of fine-grained magnesium alloys. *J. Mater. Res.* 27, 1295–1302. doi:10.1557/jmr.2012.52

Swain, M. V., and Hagan, J. T. (1976). Indentation plasticity and the ensuing fracture of glass. *J. Phys. D Appl. Phys.* 9, 2201. doi:10.1088/0022-3727/9/15/011

Trelewicz, J. R., and Schuh, C. A. (2008). The Hall–Petch breakdown at high strain rates: optimizing nanocrystalline grain size for impact applications. *Appl. Phys. Lett.* 93, 171916. doi:10.1063/1.3000655

Vogel, W. (1994). *Glass Chemistry*. Springer-Verlag.

Wheeler, J. M., and Gunner, A. G. (2013). Analysis of failure modes under nano-impact fatigue of coatings via high-speed sampling. *Surf. Coat. Technol.* 232, 264–268. doi:10.1016/j.surfcoat.2013.05.028

Winterstein-Beckmann, A., Möncke, D., Palles, D., Kamitsos, E. I., and Wondraczek, L. (2014a). A Raman-spectroscopic study of indentation-induced structural changes in technical alkali-borosilicate glasses with varying silicate network connectivity. *J. Non Cryst.' Solids* 405, 196–206. doi:10.1016/j.jnoncrysol.2014.09.020

Winterstein-Beckmann, A., Möncke, D., Palles, D., Kamitsos, E. I., and Wondraczek, L. (2014b). Raman spectroscopic study of structural changes induced by micro-indentation in low alkali borosilicate glasses. *J. Non Cryst. Solids* 401, 110–114. doi:10.1016/j.jnoncrysol.2013.12.038

Yano, T., Kunimine, N., Shibata, S., and Yamane, M. (2003a). Structural investigation of sodium borate glasses and melts by Raman spectroscopy. II. Conversion between BO4 and BO2O- units at high temperature. *J. Non Cryst. Solids* 321, 147–156. doi:10.1016/S0022-3093(03)00159-5

Yano, T., Kunimine, N., Shibata, S., and Yamane, M. (2003b). Structural investigation of sodium borate glasses and melts by Raman spectroscopy. III. Relation between the rearrangement of super-structures and the properties of glass. *J. Non Cryst. Solids* 321, 157–168. doi:10.1016/S0022-3093(03)00160-1

Yao, Z. Y., Möncke, D., Kamitsos, E. I., Houizot, P., Célarié, F., Rouxel, T., et al. (2016). Structure and mechanical properties of copper–lead and copper–zinc borate glasses. *J. Non Cryst. Solids* 435, 55–68. doi:10.1016/j.jnoncrysol.2015.12.005

Yoshida, S., Sangleboeuf, J.-C., and Rouxel, T. (2005). Quantitative evaluation of indentation-induced densification in glass. *J. Mater. Res.* 20, 3404–3412. doi:10.1557/jmr.2005.0418

Youn, S. W., and Kang, C. G. (2005). FEA study on nanodeformation behaviors of amorphous silicon and borosilicate considering tip geometry for pit array fabrication. *Mater. Sci. Eng. A* 390, 233–239. doi:10.1016/j.msea.2004.08.041

Zhang, L., and Eckert, H. (2008). Influence of phosphate precursors on the structures of sodium aluminophosphate sols, gels and glasses. *J. Non Cryst. Solids* 354, 1331–1337. doi:10.1016/j.jnoncrysol.2006.10.089

Conflict of Interest Statement: The authors declare that the research was conducted in the absence of any commercial or financial relationships that could be construed as a potential conflict of interest.

Copyright © 2017 Zehnder, Bruns, Peltzer, Durst, Korte-Kerzel and Möncke. This is an open-access article distributed under the terms of the Creative Commons Attribution License (CC BY). The use, distribution or reproduction in other forums is permitted, provided the original author(s) or licensor are credited and that the original publication in this journal is cited, in accordance with accepted academic practice. No use, distribution or reproduction is permitted which does not comply with these terms.